Molecular Therapy
Nucleic Acids
Original Article

Tissue pharmacokinetics of antisense oligonucleotides

Erica Bäckström,[1] Alessandro Bonetti,[2] Per Johnsson,[2] Stefan Öhlin,[3] Anders Dahlén,[2] Patrik Andersson,[4] Shalini Andersson,[2] and Peter Gennemark[5,6]

[1]Drug Metabolism and Pharmacokinetics, Research and Early Development, Respiratory & Immunology (R&I), BioPharmaceuticals R&D, AstraZeneca, 431 83 Gothenburg, Sweden; [2]Oligonucleotide Discovery, Discovery Sciences, BioPharmaceuticals R&D, AstraZeneca, 431 83 Gothenburg, Sweden; [3]Business, Planning Operations, Clinical Pharmacology and Safety Sciences, BioPharmaceuticals R&D, AstraZeneca, 431 83 Gothenburg, Sweden; [4]Safety Innovation, Safety Sciences, Clinical Pharmacology and Safety Sciences, BioPharmaceuticals R&D, AstraZeneca, 431 83 Gothenburg, Sweden; [5]Drug Metabolism and Pharmacokinetics, Research and Early Development, Cardiovascular, Renal and Metabolism (CVRM), BioPharmaceuticals R&D, AstraZeneca, 431 83 Gothenburg, Sweden; [6]Department of Biomedical Engineering, Linköping University, 581 85 Linköping, Sweden

Pharmacokinetics (PK) of antisense oligonucleotides (ASOs) is characterized by rapid distribution from plasma to tissue and slow terminal plasma elimination driven by re-distribution from tissue. Quantitative understanding of tissue PK and RNA knockdown for various ASO chemistries, conjugations, and administration routes is critical for successful drug discovery. Here, we report concentration-time and RNA knockdown profiles for a gapmer ASO with locked nucleic acid ribose chemistry in mouse liver, kidney, heart, and lung after subcutaneous and intratracheal administration. Additionally, the same ASO with liver targeting conjugation (galactosamine-*N*-acetyl) is evaluated for subcutaneous administration. Data indicate that exposure and knockdown differ between tissues and strongly depend on administration route and conjugation. In a second study, we show that tissue PK is similar between the three different ribose chemistries locked nucleic acid, constrained ethyl and 2′-*O*-methoxyethyl, both after subcutaneous and intratracheal administration. Further, we show that the half-life in mouse liver may vary with ASO sequence. Finally, we report less than dose-proportional increase in liver concentration in the dose range of 3–30 μmol/kg. Overall, our studies contribute pivotal data to support design and interpretation of ASO *in vivo* studies, thereby increasing the probability of delivering novel ASO therapies to patients.

INTRODUCTION

An antisense oligonucleotide (ASO) is a single-stranded ribonucleotide therapeutics, typically 16–20 nucleotides long, designed to bind complementary to the target RNA via Watson-Crick base pairing.[1] This binding enables specific regulation of target RNA by modulating splicing, by inhibiting or redirecting translation initiation or by degradation of the target RNA by recruiting endonuclease ribonuclease H1 (RNase H1) using so-called gapmer ASOs.[2] This work considers ASOs with the latter mechanism.

The natural unmodified DNA and RNA phosphodiester (PO) linkages in the backbone of an oligonucleotide are highly susceptible to degradation by nucleases *in vivo*. A common way to counter this degradation is to replace the PO linkages with the sulphur-containing phosphorothioate (PS) linkages (Figure 1A).[3] This replacement increases resistance to endonucleases and improves bioavailability by reducing renal clearance because of increased affinity to plasma proteins. However, the PS linkages also reduce the affinity to the target RNA.[3,4] To overcome this antagonistic effect, it is common to modify the 2′-position of the ribose of the nucleotide, e.g., by 2′-*O*-(2-methoxyethyl) (2′-MOE) modification (Figure 1B).[4] Other reported modifications include two conformationally constrained analogues; locked nucleic acid (LNA) and the more recent constrained ethyl (cEt), both containing a tether between the 2′-OH and the 4′ position of the ribose ring (Figure 1B). These modifications result in greater binding affinity.[4,5] The chimeric RNase H1-dependent oligonucleotide is generally designed with a full PS backbone and two regions (wings) of 2′-modified ribose residues on either end of the molecule that flank a central deoxyribonucleoside region without 2′ ribose modifications, referred to as a gap. This gap supports RNase H1 activity leading to enzymatic cleavage of the complementary bound RNA.[6] To further improve ASO drug properties it is common to modify the cytosine base to 5-methylcytosine (Figure 1C) to decrease immunogenic responses.

Pharmacokinetics (PK) of ASOs, mostly studied for 2′-MOE ribose chemistry, is characterized by a rapid distribution from plasma to tissue and a slow terminal plasma half-life driven by re-distribution from tissue.[7,8] ASOs administered systemically distribute broadly to various tissues, predominately to liver, kidney, bone marrow, adipocytes, and lymph nodes.[8] The tissue half-life is in the order of one week in mouse and several weeks in monkey and human.[9] Quantitative understanding of tissue PK and pharmacodynamics (PD) in

Received 11 May 2023; accepted 30 January 2024;
https://doi.org/10.1016/j.omtn.2024.102133.

Correspondence: Peter Gennemark, Drug Metabolism and Pharmacokinetics, Research and Early Development, Cardiovascular, Renal and Metabolism (CVRM), BioPharmaceuticals R&D, AstraZeneca, 431 83 Gothenburg, Sweden.
E-mail: peter.gennemark@astrazeneca.com

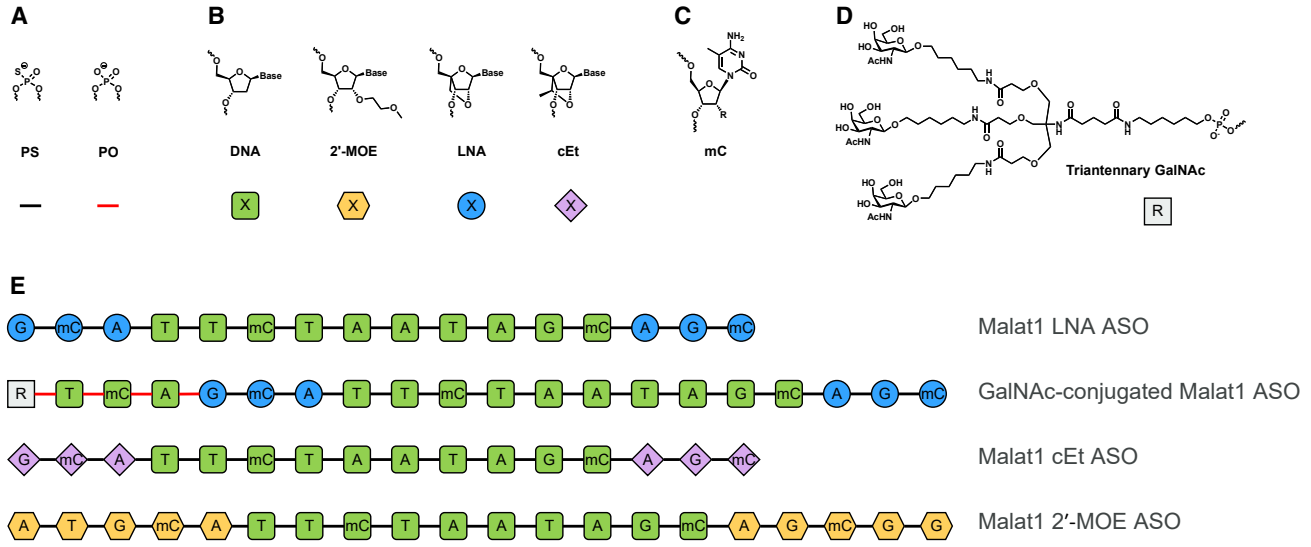

Figure 1. ASO chemistry and main sequences used in the presented studies

(A) PS and PO linkers. (B) Standard DNA and common 2′-ribose modifications. The "base" group can be either of adenine (A), guanine (G), thymine (T), cytosine (C), or 5-methylcytosine (mC). (C) Base modification in form of mC. (D) Triantennary GalNAc. (E) Malat1 LNA ASO, GalNAc-conjugated Malat1 LNA ASO, Malat1 cEt ASO, and Malat1 2′-MOE ASO gapmers with PS backbone. The coding in form of color and shape is defined in (A–D).

form of target RNA knockdown for various ASO chemistries, with and without conjugates, and for various administration routes, is critical for efficient ASO drug discovery. Conjugation of triantennary galactosamine-*N*-acetyl (GalNAc) (Figure 1D) to the ASO promotes liver uptake via the asialoglycoprotein receptor primarily expressed on hepatocytes, resulting in 10- to 30-fold increased potency in isolated hepatocytes, in *in vivo* animal models[10–12] and in the clinic.[12,13]

Here, we present mouse PK data of ASOs for two routes of administration, subcutaneous (SC) and intratracheal (IT). The first is commonly used both in preclinical and clinical drug discovery and development. The second introduces a substance directly into the trachea with main uptake via the lungs. Generally, the lungs can be reached by direct administration (inhalation or IT) or indirectly via systemic delivery as the entire cardiac output passes the peripheral part of the lung where the gas exchange takes place. IT administration is often used in preclinical studies as a surrogate to inhalation because significantly less amount of compound is required, and less advanced equipment is needed.

Specifically, we present densely sampled concentration-time and RNA knockdown profiles for an LNA gapmer ASO targeting long non-coding RNA metastasis associated lung adenocarcinoma transcript 1 (*Malat1*; Figure 1E) in mouse liver, kidney, heart, and lung after SC and IT administration. Additionally, the same ASO with triantennary GalNAc-conjugation for improved hepatocyte targeting is evaluated for SC administration (Figure 1E). Furthermore, we investigate tissue PK and RNA knockdown after SC and IT administration of non-conjugated Malat1 ASO with three different ribose chemistries (LNA, cEt, 2′-MOE) (Figure 1E). Finally, we present data on how the nucleobase sequence of gapmer ASOs with LNA chemistry affects tissue PK properties, and on the linearity of tissue PK for gapmer ASOs. The data presented here support design and interpretation of ASO *in vivo* studies and increase the probability of delivering novel ASO therapies to patients.

RESULTS

Temporal tissue PK and RNA knockdown after SC administration of Malat1 LNA ASO

We collected densely sampled ASO concentration and *Malat1* lncRNA knockdown time profiles (6 h to 4 weeks) in mouse liver, kidney, heart and lung after single-dose SC administration of Malat1 LNA ASO (4.7 μmol/kg, 25 mg/kg) and Malat1 GalNAc-conjugated LNA ASO (0.64 μmol/kg, 5.0 mg/kg of the conjugated ASO) (Figure 2 and Table 1). The dose levels were chosen to result in similar *Malat1* lncRNA knockdown in the liver. The tissue elimination rates were roughly constant over time in all tissues, and independent on conjugation, with tissue half-lives in the range of 110–190 h. Non-conjugated ASO concentrations in kidney and liver were at least one order of magnitude greater than in heart and lung. For Malat1 LNA ASO, maximum *Malat1* lncRNA knockdown observed at day 7 was 85%, 60%, 23%, and 52% in the liver, kidney, heart, and lung, respectively. For GalNAc-conjugated Malat1 LNA ASO, the corresponding maximum knockdown at day 7 was 83%, 36%, 13%, and 25% in the liver, kidney, heart, and lung, respectively.

As expected, the liver exposure was greater, about 3.5-fold for dose-normalized area under the curve (AUC), for GalNAc-conjugated ASO compared with non-conjugated ASO (Table 1). The kidney exposure shifted in the opposite direction and was about 13% lower

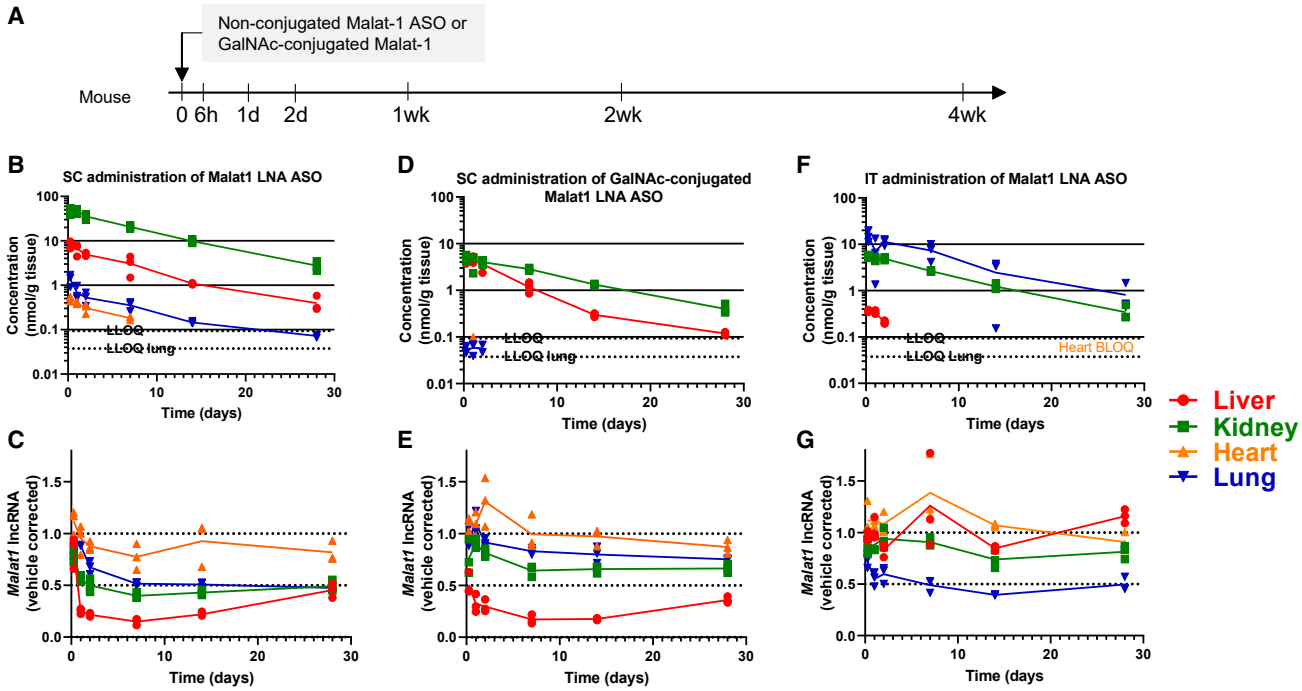

Figure 2. Time profiles of compound concentration and *Malat1* lncRNA knockdown in liver, kidney, heart and lung in mouse after SC administration of non-conjugated Malat1 LNA ASO or GalNAc-conjugated Malat1 LNA ASO, or after IT administration of non-conjugated Malat1 LNA ASO (N = 3 per time point)

Each datapoint represents one animal and the lines represent the mean trajectory. (A) The study design in which mice were administered a single SC or IT ASO dose and euthanized for measurements of tissue exposure and *Malat1* lncRNA knockdown at indicated time points. (B and C) Tissue PK and *Malat1* lncRNA knockdown in the various tissues after SC administration of 4.7 μmol/kg (25 mg/kg) non-conjugated Malat1 LNA ASO. (D and E) Tissue PK and *Malat1* lncRNA knockdown in the various tissues after SC administration of 0.64 μmol/kg (5.0 mg/kg) GalNAc-conjugated Malat1 LNA ASO. (F and G) Tissue PK and knockdown in the various tissues after IT administration of 0.19 μmol/kg (1.0 mg/kg) non-conjugated Malat1 LNA ASO. All heart concentrations were below the lower limit of quantification (LLOQ). For all tissue concentration (B, D, F), the unconjugated ASO form was measured, and the dotted lines indicate the LLOQ.

with GalNAc-conjugation compared with the non-conjugated form. Despite the 7-fold difference in amount of dose and ∼2-fold difference in liver concentration, the RNA knockdown in the liver was similar between GalNAc-conjugated and non-conjugated ASO, likely reflecting the targeting effect and the improved productive uptake using GalNAc conjugation.

Finally, we compared tissue concentration data for non-conjugated Malat1 LNA ASO with corresponding data sampled at 48 and 168 h after a single SC dose in a previous study from the same laboratory and we conclude that study-study variability is low (Figure S1).

Temporal tissue PK and RNA knockdown after IT administration of Malat1 LNA ASO

We next investigated the mouse tissue PK and *Malat1* lncRNA knockdown after a single IT-administrated dose of the same non-conjugated Malat1 LNA ASO (0.19 μmol/kg, 1.0 mg/kg) that was used in the studies with SC administration. The dose level was chosen to result in similar *Malat1* lncRNA knockdown in the lung as for SC administration of the same compound. Densely sampled ASO concentration and RNA knockdown time profiles were collected from liver, kidney, heart, and lung (Figure 2 and Table 1). The tissue half-lives could be determined in kidney and lung and were approximately 160 h, similar to what was observed after SC administration. After IT administration of Malat1 LNA ASO, tissue concentration was greatest in lung, followed by kidney and liver, while the heart concentration was below the limit of quantification. *Malat1* lncRNA knockdown was observed in the lung already after 24 h, and maximum knockdown of 17%, 26%, and 60% in the liver, kidney, and lung, respectively, was observed at day 14. No major knockdown was observed in the heart.

The tissue concentration data for non-conjugated Malat1 LNA ASO were compared with corresponding data sampled at 48 and 168 h after a single IT dose in a previous study from the same laboratory and we conclude that study-study variability is relatively low (Figure S1).

Tissue PK and RNA knockdown after SC administration of non-conjugated Malat1 ASO with various chemistries

We next investigated the impact on tissue PK and lncRNA knockdown by Malat1 ASOs with the following ribose chemistries and number of nucleotides: LNA (16mer), cEt (16mer), and 2′-MOE

Table 1. Estimated PK and *Malat1* lncRNA knockdown parameters for liver, kidney, heart and lung after SC administration of non-conjugated Malat1 LNA ASO (upper part) and GalNAc-conjugated Malat1 LNA ASO (middle part), and after IT administration of non-conjugated Malat1 LNA ASO (lower part)

	Liver	Kidney	Heart	Lung
LNA Malat1, single SC dose of 4.7 μmol/kg				
T_{max} (h)	6	24	6	6
C_{max} (nmol/g tissue), mean (SE)	8.62 (0.94)	47.8 (3.8)	0.504 (0.037)	1.37 (0.24)
AUC (nmol/g tissue × h) Point estimate (5th and 95th percentiles)	1,400 (1,200, 1,600)	9,970 (9,200, 11,000)	90.6 (73, 110)	183 (150, 230)
Tissue half-life (h) PE (5th and 95th percentiles)	152 (120, 180)	161 (140, 180)	188 (130, 220)	179 (130, 210)
C_{max}/dose (nmol/g tissue/μmol/kg)	1.8	10	0.11	0.29
AUC/dose (nmol/g tissue × h/μmol/kg)	300	2,100	19	39
Malat1 lncRNA max reduction (%), mean (SE)	85.1 (1.8)	60.2 (1.7)	22.6 (7.2)	52.5 (1.9)
Malat1 lncRNA reduction at 4 weeks (%), mean (SE)	54.6 (4.0)	50.9 (3.1)	18.2 (5.7)	52.5 (1.9)
GalNAc-conjugated LNA Malat1, single SC dose of 0.64 μmol/kg				
T_{max} (h)	24	6	[a]	24
C_{max} (nmol/g tissue), mean (SE)	4.79 (0.45)	4.73 (0.50)	[a]	0.0583 (0.010)
AUC (nmol/g tissue × h) Point estimate (5th and 95th percentiles)	664 (580, 770)	1,170 (1,000, 1,300)	[a]	[a]
Tissue half-life (h) PE (5th and 95th percentiles)	110 (90, 130)	188 (170, 220)	[a]	[a]
C_{max}/Dose (nmol/g tissue)/μmol/kg)	7.5	7.4	[a]	0.091
AUC/Dose (nmol/g tissue × h/μmol/kg)	1,040	1,830	[a]	[a]
Malat1 lncRNA max reduction (%), mean (SE)	82.9 (2.5)	35.8 (3.0)	13 (3.8)	24.8 (0.4)
Malat1 lncRNA reduction at 4 weeks (%), mean (SE)	64.1 (1.8)	33.6 (2.4)	13 (3.8)	24.8 (0.4)
LNA Malat1, single IT dose of 0.19 μmol/kg				
T_{max} (h)	6	6	[a]	6
C_{max} (nmol/g tissue), mean (SE)	0.366 (0.011)	5.47 (0.25)	[a]	15.2 (2.5)
AUC (nmol/g tissue × h) Point estimate (5th and 95th percentiles)	[a]	1,220 (1,100, 1,300)	[a]	2,210 (1,400, 3,100)
Tissue half-life (h) PE (5th and 95th percentiles)	[a]	162 (140, 180)	[a]	159 (110, 210)
C_{max}/dose (nmol/g tissue)/μmol/kg)	1.9	29	[a]	80
AUC/dose (nmol/g tissue × h/μmol/kg)	[a]	6,400	[a]	12,000
Malat1 lncRNA max reduction (%), mean (SE)	17.0 (3.6)	26.2 (5.0)	9.2 (5.1)	60.5 (0.3)
Malat1 lncRNA reduction at 4 weeks (%), mean (SE)	−15.9 (3.8)	18.7 (3.7)	9.2 (5.1)	50.5 (3.8)

The ASOs have full PS backbone chemistry. The AUC estimates are for the time interval 0 to 4 weeks.
C_{max}, maximum concentration; LNA, locked nucleic acid; PE, point estimate; SE, standard error; T_{max} , time of C_{max}.
[a]The majority of PK samples below the lower limit of quantification.

(20mer). To make the comparison as fair as possible, the three ASOs were designed with nucleobase sequences targeting the same part of *Malat1* lncRNA. However, because the lengths of the ASOs differ (c.f., Figure 1), the intrinsic potency of the ASOs may differ and result in differences in lncRNA knockdown.

Mice were SC administered a single dose of ASO and euthanized either 2 or 7 days after dosing with N = 3 per time point. The study was designed with equal doses on amount (μmol/kg) scale. The tissue distribution pattern was similar between the three chemistries with highest concentration in the kidney, followed by liver, lung, and heart (Figures 3A–3C and Table 2). Data indicate that cEt chemistry results in lower liver concentration ($p < 0.05$ at day 2 and $p < 0.001$ at day 7) compared with the two other chemistries. In the kidneys, 2′-MOE chemistry results in lower concentration ($p < 0.01$ at days 2 and 7) compared with LNA chemistry, and trends to be smaller compared with cEt chemistry ($p < 0.01$ at 2; not significant at day 7). In the heart, cEt chemistry results in lower concentration compared with both LNA and 2′-MOE chemistries ($p < 0.05$) at day 2, and to 2′-MOE chemistry ($p < 0.01$) at day 7. LNA chemistry trends to result in

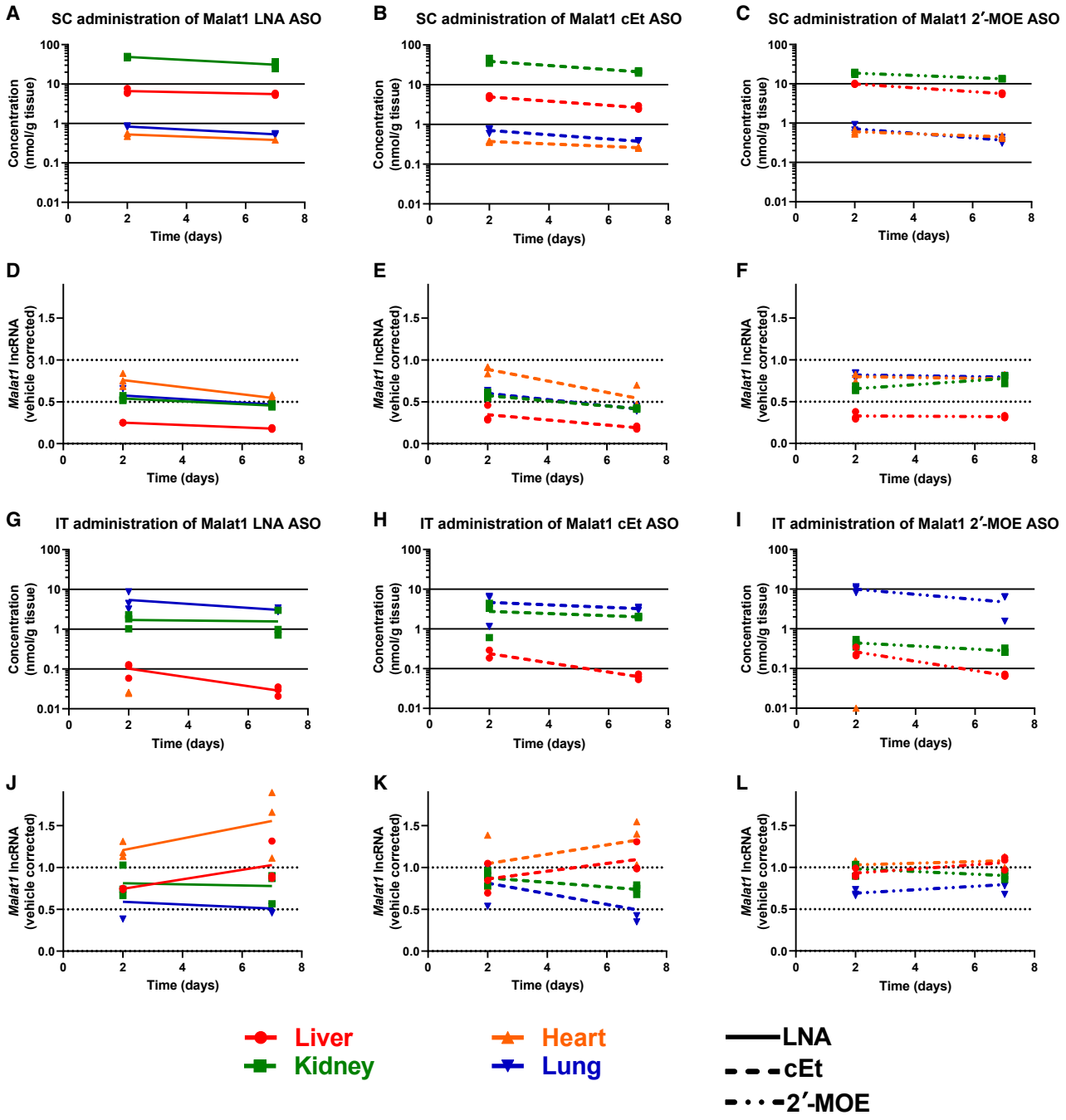

Figure 3. Compound concentration and *Malat1* lncRNA knockdown in liver, kidney, heart and lung in mouse after SC or IT administration of non-conjugated Malat1 ASO with full PS backbone and various chemistries (N = 3 per time point)

Each datapoint represents one animal and the lines represent the mean trajectory. (A–C) Tissue concentration after SC administration in the various tissues for LNA chemistry (4.7 μmol/kg, ∼25 mg/kg) (A), cEt chemistry (4.6 μmol/kg, ∼25 mg/kg) (B) and 2′-MOE chemistry (4.7 μmol/kg, ∼34 mg/kg) (C). All samples were above the lower limit of quantification. (D–F) Knockdown of *Malat1* lncRNA in the various tissues for LNA (D), cEt (E), and 2′-MOE (F) chemistry after SC administration. (G–I) Tissue concentration after IT administration in the various tissues for LNA chemistry (0.20 μmol/kg, ∼1.1 mg/kg) (G), cEt chemistry (0.20 μmol/kg, ∼1.1 mg/kg) (H), and 2′-MOE chemistry (0.20 μmol/kg, ∼1.4 mg/kg) (I). Most heart samples were below the lower limit of quantification. (J–L) Knockdown of *Malat1* lncRNA in the various tissues for LNA (J), cEt (K), and 2′-MOE (L) chemistry after IT administration.

Table 2. Estimated PK and *Malat1* lncRNA knockdown parameters for liver, kidney, heart and lung after SC (upper part) and IT (lower part) administration of non-conjugated Malat1 LNA ASO

SC admin	LNA Malat1 (4.7 μmol/kg)				cEt Malat1 (4.6 μmol/kg)				2′-MOE Malat1 (4.7 μmol/kg)			
	Liver	Kidney	Heart	Lung	Liver	Kidney	Heart	Lung	Liver	Kidney	Heart	Lung
C at 48 h (nmol/g tissue), mean (SE)	6.61 (0.58)	48.7 (1.2)	0.526 (0.029)	0.837 (0.015)	4.92 (0.23)	38.8 (3.8)	0.372 (0.0092)	0.703 (0.056)	9.93 (0.24)	18.8 (0.70)	0.603 (0.048)	0.716 (0.11)
C at 168 h (nmol/g tissue), mean (SE)	5.55 (0.21)	31.0 (3.7)	[a]	0.532 (0.014)	2.67 (0.17)	21.2 (0.86)	0.260 (0.0070)	0.379 (0.0056)	5.65 (0.17)	13.5 (0.088)	0.450 (0.022)	0.370 (0.037)
Tissue half-life (h) PE (95% CI)	494 (194, inf)	179 (103, 710)	[a]	183 (153, 226)	135 (100, 211)	139 (94, 262)	233 (182, 326)	136 (98, 221)	147 (124, 181)	252 (190, 372)	288 (152, inf)	128 (73, 525)
Malat1 lncRNA reduction at 48 h (%), mean (SE)	75.0 (0.19)	46.1 (1.8)	24.1 (4.5)	42.5 (4.2)	65.4 (5.6)	42.6 (2.2)	11.2 (2.6)	39.9 (1.8)	67.2 (2.7)	34.5 (1.7)	20.1 (2.8)	18.0 (2.2)
Malat1 lncRNA reduction at 168 h (%), mean (SE)	82.0 (0.55)	54.5 (1.1)	45.3 (2.4)	53.2 (0.49)	81.0 (1.1)	58.1 (0.57)	45.6 (7.7)	58.3 (1.7)	68.0 (0.78)	22.4 (3.1)	22.6 (2.6)	20.6 (1.1)
IT admin	**LNA Malat1 (0.20 μmol/kg)**				**cEt Malat1 (0.20 μmol/kg)**				**2′-MOE Malat1 (0.20 μmol/kg)**			
	Liver	**Kidney**	**Heart**	**Lung**	**Liver**	**Kidney**	**Heart**	**Lung**	**Liver**	**Kidney**	**Heart**	**Lung**
C at 48 h (nmol/g tissue), mean (SE)	0.102 (0.022)	1.71 (0.37)	0.0252 (0.00080)	5.44 (1.6)	0.238 (0.054)	2.77 (1.1)	[a]	4.64 (1.8)	0.261 (0.043)	0.441 (0.055)	0.00778 (0.0011)	10.0 (0.98)
C at 168 h (nmol/g tissue), mean (SE)	0.0287 (0.0043)	1.56 (0.72)	[a]	3.06 (0.20)	0.0627 (0.0058)	2.02 (0.048)	[a]	3.26 (0.18)	0.0674 (0.0025)	0.281 (0.023)	0.00462 (0.0010)	4.74 (1.6)
Tissue half-life (h) PE (95% CI)	67 (41, 199)	352 (51, inf)	[a]	169 (63, inf)	63 (42, 126)	[b]	[a]	[b]	62 (47, 93)	188 (97, inf)	154 (69, inf)	91 (37, inf)
Malat1 lncRNA reduction at 48 h (%), mean (SE)	25.6 (0.43)	18.8 (11)	−20.8 (5.3)	40.9 (10)	13.8 (10)	12.3 (5.2)	−4.51 (18)	18.7 (14)	6.79 (3.0)	1.67 (4.5)	−2.95 (4.4)	30.9 (2.1)
Malat1 lncRNA reduction at 168 h (%), mean (SE)	−2.82 (14)	22.2 (11)	−55.6 (23)	49.2 (2.6)	−9.47 (11)	26.1 (3.3)	−32.6 (15)	50.6 (11)	−5.64 (4.6)	9.77 (2.9)	−7.86 (4.0)	20.7 (7.2)

The ASOs have full PS backbone and either LNA, cEt or 2'-MOE ribose chemistry.
2′-MOE, methoxyethylribose; C, concentration; CI, confidence interval; LNA, locked nucleic acid; PE, point estimate; inf, infinity; SE, standard error.
[a]The majority of PK samples below the lower limit of quantification.
[b]No half-life calculated because of the slight increase in concentration over time, or very large spread in data between animals at specific time points.

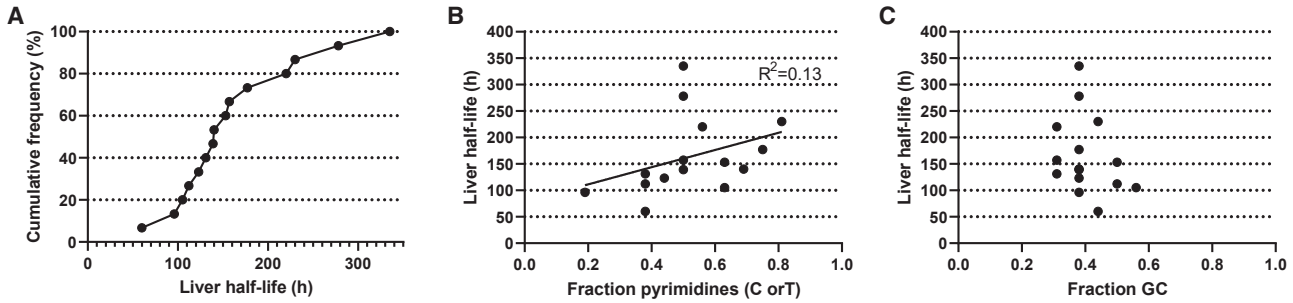

Figure 4. Estimated liver half-lives for 15 non-conjugated ASOs with the same LNA chemistry and all targeting the same gene

(A) Distribution of half-lives in the liver. (B) Correlation between liver half-life and fraction of pyrimidines in the ASO sequence. (C) Correlation between liver half-life and GC content of the ASO sequence.

greater lung concentrations ($p < 0.01$ at day 7; not significant at day 2) compared with the other two chemistries.

Generally, across ribose chemistries, data on *Malat1* lncRNA indicate greatest knockdown of 70%–80% at day 7 in the liver, followed by kidney and lung with 20%–60% knockdown at day 7, and with the smallest knockdown of 20%–45% observed in the heart (Figures 3D–3F and Table 2). Furthermore, data indicate a relatively similar knockdown for LNA and cEt chemistries, while 2′-MOE chemistry generally results in less knockdown compared with the former two. Specifically, the 2′-MOE chemistry leads to less knockdown in kidney (trending at day 2, and $p < 0.001$ at day 7), liver ($p < 0.001$ at day 7) and lung ($p < 0.01$ at day 2 and $p < 0.001$ at day 7), and heart ($p < 0.05$ at day 7), compared with the other two chemistries. One possible reason for the difference in knockdown is a difference in intrinsic potency.

We note the disconnect between tissue concentration and knockdown. For example, the kidney is more exposed than the liver, but knockdown in the kidney is lower compared with liver likely because of lower productive uptake resulting in knockdown.

Tissue PK and RNA knockdown after IT administration of non-conjugated Malat1 ASO with various chemistries

The tissue PK and target knockdown profiles were compared for three ASOs with different ribose chemistries after IT administration of a single dose to mice. The study was designed with equal doses on amount (μmol/kg) basis. Tissue PK appears roughly similar between the three chemistries with highest concentration in the lung, followed by kidney and liver, while heart is below the lower limit of quantification (Figures 3G–3I and Table 2). Data indicate that the LNA chemistry trends to a lower liver concentration ($p < 0.01$ at day 7; not significant at day 2) compared with the two other chemistries. No other major differences between the chemistries were observed. Data on *Malat1* lncRNA knockdown indicate no significant differences between the three chemistries (Figures 3J–3L). Greatest knockdown of 20%–50% was observed in lung at day 7, followed by kidney at about 10%–30% knockdown. The 2′-MOE chemistry trends to less knockdown in lung tissue at day 7 compared with the two other chemistries.

Sequence aspects on PK properties of non-conjugated ASOs with LNA chemistry

We next investigated the liver half-life in the mouse for a larger cohort of 15 gapmer ASOs targeting the same gene and having full PS and LNA chemistry. To this end, we collected liver concentration-time data (2 and 7 days; N = 3 per time point) after SC administration at a dose level of 25 mg/kg. The full PK profiles are given in Figure S2. Data indicate that half-life varies with sequence with a median point estimate of 140 h and with 90% of the sequences having point estimates in interval [70, 240 h] (Figure 4A). Furthermore, the data indicate a small positive linear association (with correlation $R^2 = 0.13$) between *in vivo* liver half-life and the pyrimidine/purine ratio of the ASO (Figure 4B). Finally, we observed no correlation ($R^2 < 0.1$) between the fraction of G or C residues in the ASO sequence and the liver half-life (Figure 4C).

Linearity of liver PK in the mouse

Finally, we investigated linearity of liver PK by comparing single doses at 25 mg/kg (3–5 μmol/kg depending on molecular weight) in female C57 BL6/J mice and 150 mg/kg (20–30 μmol/kg) in male and female Balb/c mice for a set of nine ASO with varying chemistries. For LNA and 2′-MOE chemistries, we observed less than dose-proportional increase in liver concentration between the low dose and the high dose (Figure 5). Specifically, the population marginal means of the low-dose groups and the high-dose groups were significantly different ($p < 10^{-13}$ for LNA and $p < 10^{-6}$ for 2′-MOE). The sparse cEt data trends in the same direction as for the other two chemistries.

DISCUSSION

We have presented concentration and lncRNA knockdown time profiles for a Malat1 gapmer ASO with LNA chemistry in various tissues of the mouse for SC and IT administration. Additionally, the same ASO with liver-targeting GalNAc-conjugation was evaluated for SC administration. Data indicate that exposure and knockdown differ between tissues and strongly depends on administration route and conjugation. The relationship between PK and lncRNA knockdown also differs between tissues due to varying degrees of uptake leading to PD effect, e.g., lncRNA knockdown in the desired cell type within the tissue. The choice of *Malat1* as target gene is adequate for the

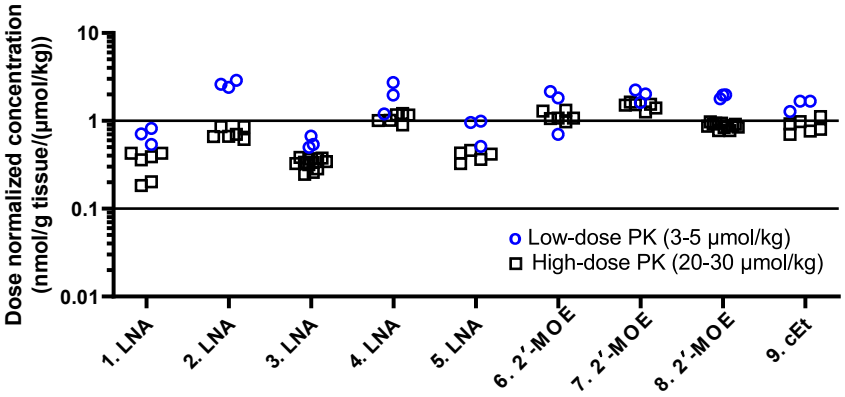

Figure 5. Comparison of dose-normalized liver concentrations in mouse at 72 h after dosing at two different dose levels: 25 mg/kg (3–5 μmol/kg depending on molecular weight) and 150 mg/kg (20–30 μmol/kg)

The latter data come from a high-dose PK study after SC administration with termination at 72 h (N = 12 for number 3 and 8, and N = 6 per compound for all other). The low-dose data come from a mouse single-dose PK study after SC administration, with predicted liver concentration at 72 h based on measured concentrations at 48 h and 168 h and a log-linear slope (N = 3 per compound).

presented benchmark studies, because *Malat1* lncRNA is expressed at high levels in most cell types.[14] In a second study, we showed that tissue PK is similar between three ASOs with different ribose modifications (LNA, cEt, and 2′-MOE) after SC and IT administration. Further, we showed that the half-life in mouse liver may vary with ASO sequence. Finally, we reported a less than dose-proportional increase in liver concentration in the dose range 3–30 μmol/kg. We now discuss each of the presented datasets more in depth.

Temporal tissue PK and RNA knockdown after SC administration of Malat1 LNA ASO

The study was designed for a relevant comparison of non-conjugated and GalNAc-conjugated ASOs at similar knockdown in the most relevant tissue, namely, liver. The 7-fold difference in amount of dose, with lower dose for conjugated ASOs compared with non-conjugated ASOs, resulted in an approximately similar knockdown in liver (red markers and lines in Figures 2C and 2E), confirming that the design was appropriate. The reported data are in agreement with previous data from Geary et al., who compare tissue parent (20-gapmer) oligonucleotide concentrations at 24 h after a single intravenous administration at a dose of 3 mg/kg across species for a representative chimeric 2′-MOE ASO.[7] He reports liver and kidney concentrations of 16 and 61 μg/g tissue in mouse and of 101 and 145 μg/g tissue in monkey. The kidney-to-liver ratio of 3.8 in mouse aligns relatively well with the corresponding ratio of 5.5 at a maximum concentration for non-conjugated Malat1 LNA based on data in Table 1.

We note that tissue concentration is not directly related to RNA knockdown when compared across tissues. For example, the kidney concentration is highest among the tissues analyzed, but the knockdown is greater in the liver compared with the kidney. We speculate that this could be due to differences in the so-called productive and non-productive uptake,[15,16] as well as variation in cell-type specific uptake and expression of the targeted RNA.

Temporal tissue PK and RNA knockdown after IT administration of Malat1 LNA ASO

The single-dose IT administration study was designed to result in similar lncRNA knockdown in the most relevant tissue, namely, lung, as after single-dose SC administration. In this way, the study provides a relevant comparison of non-conjugated ASOs between the two routes of administration. The 25-fold difference in dose, with lower dose for IT administration compared with SC administration, resulted in approximately similar knockdown in the lung (blue markers and lines in Figures 2C and 2G), confirming that the design was appropriate. Notably, the chosen IT dose level is not considered to cause infiltration of inflammatory cells.

Data on lung tissue half-life (7 days) in mice after IT delivery in the present study agree with estimated mouse lung tissue half-life of 9 days after a single inhaled dose of fully PS 2′-MOE 20-gapmer.[17] Crosby et al.[18] reported a lung tissue half-life of 13 days of a fully PS cEt 16-gapmer. The greater half-life in the latter study may partly be due to the different chemistry and partly to the dosing schedules; three inhaled doses in the latter study compared with single doses in the two former studies.

While several reports consistently suggest higher exposure in kidney than lung of fully PS LNA gapmers after IT administration,[19] there is a disagreement on the relative concentration in liver compared with lung (liver > lung in Moschos et al.[19]; lung > liver in Shin et al.[20]). We notice, however, that the day of termination is different (2 days[19] vs. 7 days[20]). In contrast with these reports, we report the highest concentration in lung followed by kidney and liver (Figure 2F) across all time points after a single IT delivered dose (approximately one-half the dose used in ref.[19,20]). The present data agree with the ranking of tissue exposure reported for inhaled fully PS 2′-MOE gapmer in mice and cynomolgus monkeys (both single and repeated dosing)[17] and fully PS 2′F arabinose nucleic acid ASO in cynomolgus monkeys (repeated dosing).[21] In a study by Beumer et al.[21] with orotracheal delivery to mice, a 2′OMe steric blocking ASO had the highest ASO exposure in lung followed by similar exposure in kidney and liver.[22]

The dose level could have a major impact on the systemic exposure following direct lung delivery (IT or inhalation). Fey et al.[17] reported that disposition of an inhaled fully PS 2′-MOE 20-gapmer in lung and

Table 3. ASOs used in the presented studies

Name	Target	Gapmer structure	2′-Ribose chemistry	Backbone chemistry	Molecular weight (g/mol)
ASO to describe PK in tissues (Figures 2 and 3)					
Malat1 LNA ASO	Malat1	3-10-3	LNA	full PS	5330.3
GalNAc-conjugated Malat1 LNA ASO	Malat1	3-10-3	LNA	full PS	7770,6
Malat1 cEt ASO	Malat1	3-10-3	cEt	full PS	5414.5
Malat1 2′-MOE ASO	Malat1	5-10-5	2′-MOE	full PS	7274.1
ASOs to describe the spread in liver half-lives in the mouse (Figure 4)					
1–15		3-10-3	LNA	Full PS	
ASOs used in to describe linearity of liver PK (Figure 5)					
1		3-10-3	LNA	full PS	5341.4
2		3-10-3	LNA	full PS	5387.4
3		3-8-3	LNA	full PS	4647.8
4		3-10-3	LNA	full PS	5337.3
5		3-8-3	LNA	full PS	4661.8
6		5-10-5	2′-MOE	full PS	7226.2
7		4-10-4	2′-MOE	full PS	6404.4
8		5-10-5	2′-MOE	full PS	7165.1
9		3-10-3	cEt	full PS	5421.5

LNA, locked nucleic acid; 2′-MOE, methoxyethylribose; PS, phosphorothioate.

kidney of cynomolgus monkey was dose dependent, but not dose proportional. The concentrations in kidney at a low dose (0.5 mg/kg) were approximately 25-fold lower than in lung, whereas at a high dose (15 mg/kg) the kidney concentrations were only 2.5-fold lower as compared with lung.[23] Similarly, Nicklin et al.[23] reported increased systemic bioavailability by pulmonary administration with increased doses of a fully PS ASO, ranging from 3% bioavailability of a 0.06-mg/kg dose to 40% bioavailability of a 6-mg/kg dose.[17] This may reflect an increased transit from lung into the systemic circulation when high local concentrations are achieved in lung tissue.

Tissue PK and RNA knockdown after SC administration of non-conjugated Malat1 ASOs with various chemistries

For Malat1 ASO with 2′-MOE chemistry, we can compare tissue concentration data with corresponding data from Geary et al.[16] who report data for ISIS 116847, a 2′-MOE modified ASO, targeting putative protein tyrosine phosphatase (*PTEN*) mRNA. A single bolus SC dose of 60 mg/kg in mice resulted in liver concentration of about 90 μg/g tissue at 48 h after dose, corresponding to a dose-normalized concentration of 1.5 (nmol/g tissue)/(μmol/kg), assuming a molecular weight of 7,000 g/mol. Our data for 2′-MOE Malat1 dosed at 4.7 μmol/kg is similar, 2.1 (i.e., 9.97/4.7) (nmol/g tissue)/(μmol/kg) at 48 h (Table 2). Geary et al. report a liver half-life of 8 days, slightly greater than the 6-day half-life in our data for 2′-MOE Malat1 (Table 3). The minor difference in half-life may be due to different sequences, or different mouse strains, or both of those. Furthermore, Geary et al. report a time-dependent reduction in liver *PTEN* mRNA that was maximal at 48–72 h and returned to near control levels by 20 days after administration.

Furthermore, Yu et al.[24] report liver concentration of 400 μg/g tissue of a 2′-MOE ASO in tissue taken 48 h after the last dose of 25 mg/kg administered SC every 4th day over 3 months to CD-1 mice. Considering a 5-fold accumulation given the reported rodent half-life in liver of 13 days, the corresponding single dose liver concentration is estimated at 11 nmol/g tissue (for a molecular weight of 7,177 g/mol), and a dose-normalized liver concentration of 3.1 (nmol/g tissue)/(μmol/kg) which is of similar magnitude, but about 1.5-fold greater than we observed for Malat1 LNA ASO (2.1 (nmol/g tissue)/(μmol/kg); dose-normalized liver concentration data at 48 h in Table 2).

For Malat1 ASO with cEt chemistry, we can compare the tissue concentration data with corresponding data from Hung et al.[14] They reported liver, kidney, heart, and lung concentrations of 391, 575, 76, and 134 μg/g tissue, respectively, in tissues taken 24 h after the last dose of 50 mg/kg administered SC twice weekly over 4 weeks to BALB/c mice. Considering a 3- to 5-fold accumulation after repeated dosing, given our estimated half-lives in respective tissue (Table 3), the corresponding single dose-normalized liver, kidney, heart, and lung concentrations are estimated to 1.1, 8.5, 0.081, and 0.15 (nmol/g tissue)/(μmol/kg), respectively, which is 2.6, 0.5, 4.2, and 6.1 times greater than we observed for Malat1 cEt ASO (tissue concentration data at 48 h in Table 3). The difference may be because of different mouse strains, non-linear PK, uncertainty in the estimated half-lives, or a combination of those. Interestingly, the order or tissues, from highest to lowest concentration, is the same between the two studies: kidney>liver>lung>heart. Furthermore, Hung et al. reported RNA knockdown of both Malat1 2′-MOE and cEt chemistries for the same study protocol. The knockdown was greater for

cEt compared with 2′-MOE in kidney, lung, and heart, and similar in liver, and all these trends were recapitulated in our data both at 48 and 168 h (Table 3).

Overall, the presented SC data are aligned to previous literature.

Tissue PK and RNA knockdown after IT administration of non-conjugated Malat1 ASOs with various chemistries

The limited data in the literature of tissue exposure after a single IT dose does not allow for a direct comparison of the tissue concentrations of different ASO chemistries. In the present study, we observed roughly similar tissue PK between the three tested chemistries. Shin et al.[20] compared the silencing ability in lung tissue after IT delivery of fully PS ASO with 2′-MOE or LNA chemistry. The LNA ASO (90% knockdown) showed improved silencing in lung tissue compared with the 2′-MOE ASO (60% knockdown).[20] In line with this, we here observe that, despite a high concentration in lung tissue of the 2′-MOE ASO at 7 days, the target knockdown (∼20%) was less compared with that of the cEt (∼50%) and LNA (∼50%) ASOs. As mentioned, a direct comparison of target knockdown between the three tested ASOs is associated with some uncertainty because of different ASO lengths.

In general, a larger spread in data points from animals given an IT dose compared with a SC dose is expected because of the more complicated administration process that is more difficult to perform in a standardized manner.

Sequence aspects on PK properties of non-conjugated ASOs with LNA chemistry

It has been reported that, irrespective of the 2′-ribose modification incorporated, the PS moiety is the primary determinant of the PK properties of ASOs.[25] Our analysis indicates some remaining spread in liver half-lives between different sequences for non-conjugated ASOs, all with the same full PS and LNA chemistry. Such a spread in liver half-life is consistent with observations by Geary et al.[8] for two different sequences in the same 2′-MOE chemical class. Of relevance to this observation, the liver concentration *per se* has also been reported to vary for ASOs with the same LNA chemistry but different sequences.[26] Notably, our reported median half-life of 140 h is similar to the half-life of 152 h estimated for Malat1 ASO using rich time course data (Figure 1; Table 2). We acknowledge that part of the spread may be due to uncertainty in the half-life estimates.

Our data indicate a small trend that liver half-life increases with pyrimidine/purine ratio. In contrast, Crooke et al.[27] reported that pyrimidine-rich compounds seem to be metabolized to a greater extent than purine-rich oligomers *in vitro*. Potential reasons for this discrepancy include oligomer chemistry and length, target sequence, and differences between *in vitro* and *in vivo* experiments. Our data did not show any correlation between liver half-life and the fraction of G or C residues, here referred to as GC content. The GC content ranged from 3%1 to 56% in our set of ASO. This range is partly overlapping with a GC-content of 45%–65%, which has been associated with the most favorable ASO knockdown.[28] We note that the type of liver half-life data presented here can potentially be used to generate *in vitro-in vivo* relationships, for example by comparing the *in vivo* data with *in vitro* stability in mouse hepatocytes as suggested for siRNAs.[29] Such an approach can be useful for filtering out unstable ASOs in drug discovery.

Linearity of liver PK in the mouse

Finally, we investigated linearity of liver PK by comparing single SC doses for a set of nine ASO with varying chemistries. For LNA chemistry, we observed less than dose-proportional increase in liver concentration between the low dose of 3–5 μmol/kg and the high dose of 20–30 μmol/kg (roughly corresponding to 25 and 150 mg/kg) (Figure 5). A similar trend was observed for one of the ASOs with 2′-MOE chemistry (number 8 in Figure 5), but the other two (numbers 6 and 7), as well as the single ASO with cEt chemistry showed roughly dose-proportional PK. We acknowledge the following uncertainties in our analysis. First, low-dose studies were conducted in female C57 BL6/J mice, while the high-dose data originate from male Balb/c mice or, for two of the compounds, from both male and female Balb/c mice. For the two compounds with both male and female high-dose data, there is no sex difference in liver concentrations, suggesting limited uncertainty due to the difference in sex. Second, for the low-dose studies, the concentrations at 72 h are interpolated from observed data at 48 and 168 h.

A less than dose-proportional increase in liver concentration in mouse has previously been reported for a 2′-MOE ASO in the dose range from 1 to 30 mg/kg,[30] and for a cEt ASO in the dose range from 26 to 70 mg/kg.[31] For GalNAc-conjugated ASOs, it is known that a pronounced, less-than-dose-proportional increase in liver concentration occurs because of saturated liver uptake.[32–34] For a comparison with plasma PK, Edwards et al.[35] reported linear plasma PK of an ASO in the dose range of 160–640 mg in humans.

Overall, our data seem to align with the previous literature. However, because of the limitations of our studies, the results should be interpreted with some caution. More extensive investigations are needed to draw general conclusions about the dose linearity of ASOs, ideally conducted in the same strain and designed with sampling at the same time points.

Practical implications to pharma industry

We here present a rich dataset with densely sampled tissue profiles with concentrations and lncRNA knockdown for Malat1 LNA ASO. A direct comparison of GalNAc conjugation with non-conjugation for SC administration is carried out and a comprehensive dataset for IT administration is also generated. We believe these data will be highly valuable for the design of *in vivo* studies accounting for the right dose level, the right dosing frequency, the time to steady state for repeated administration, washout time at end of dosing, dose-concentration relationship, concentration to knockdown relationship, and other quantitative aspects of the tissue PK and RNA knockdown. These data also help to predict tissue concentrations

following various routes of administration. The second dataset informs on expected differences in PK for various chemistries, both for SC and IT administration. Finally, we present data across chemistries on the linearity in PK, something that is of importance when designing tolerability and toxicity studies. On a more general level, the presented data can serve as a benchmark in mouse for future extensions of methods for translation between species.[36–38]

Overall, this study supports the design and interpretation of ASO *in vivo* studies and guide compound ranking to ultimately increase the probability of delivering optimal ASO therapy to patients.

MATERIALS AND METHODS

Compounds

We targeted a long non-coding RNA gene, *Malat1* with chemically modified ASOs with or without GalNAc conjugation. *Malat1* is evolutionarily conserved among mammals at the level of primary sequence and highly expressed in many tissues.[14] The compounds used in the key studies (Figures 2 and 3) are listed in Table 3. To describe the spread in liver half-lives in the mouse, we used 15 ASOs for which we cannot reveal the sequence (Figure 4). All these ASOs were 3-10-3 gapmers with full PS and LNA chemistry (Table 3). In addition, to describe the linearity of liver PK in the mouse (Figure 5), we used nine ASOs for which key characteristics are reported in the lower part of Table 3 and sequences in Table S1.

Animals

For PK studies, female mice C57 BL6/J (Si Bei Fu Laboratory Animal Technology Co. Ltd; Vital River Laboratory Animal Technology Co., Ltd; HuaFuKang Bio-Technology Co. Ltd) of 8–10 weeks of age weighing 20–30 g were used. In an Association for Assessment and Accreditation of Laboratory Animal Care (AAALAC)-accredited animal facility in a controlled environment (20°C–25°C and 40%–70% relative humidity) with a 12-h light/12-h dark cycle. The animals had access to water and chow *ad libitum* for at least 3 days before the experiments, and enrichments in the cage such as gnaw stick and bedding material. The wellbeing for the PK studies, including body weight, of the animals was monitored twice weekly and at termination. Pharmaron's (Beijing Co., Ltd., China) Institutional Animal Care and Use Committee (IACUC) approved the studies, and the animal experiments conform to all relevant regulatory standards.

For the high-dose experiment (Figure 5), Male and female Balb/c mice were used (Orient Bio Inc.) of 8 weeks of age weighing 14–18 g for the females and 17–25 g for the males. Male animals were single housed, and the female animals were group-housed in an AAALAC-accredited animal facility in a controlled environment (20°C–26°C and 30%–70% relative humidity) with a 12-h light/12-h dark cycle. The animals had access to water and chow *ad libitum* for at least 3 days before the experiments, and enrichments in the cage such as gnaw stick and bedding material. The wellbeing for the high-dose experiment, including body weight, of the animals was monitored daily. The Korea Institute of Toxicology IACUC approved the studies, and the animal experiments conform to all relevant regulatory standards.

Drug formulation and *in vivo* phase

Formulation was prepared by dissolving the different test compounds in Dulbecco's PBS without calcium chloride and magnesium chloride (Gibco) at the appropriate concentration. The concentration of the dose solutions was checked by measuring optical density value at 260 nm in combination with the unique extinction coefficient of the ASO. The dose formulations were kept stirred at room temperature for at least 2 min before dosing.

The drugs were delivered via IT or SC administration. Doses ranging from 0.18 to 0.22 μmol/kg for IT delivery and 0.64 to 30 μmol/kg for SC delivery and the dose volumes were 2 mL/kg for IT delivery and 4 mL/kg for SC delivery. At the time of sampling, the animals were anesthetized with isoflurane (Lunan BETTER Pharmaceutical Co., Ltd.) by inhalation and the absence of ped reflex was tested before the procedure was initiated. The animals were euthanized by cutting the heart before the tissues were removed to minimize blood contamination of the tissue. Lung, liver, kidney, and heart were sampled for exposure analysis with liquid chromatography-tandem mass spectrometry (LC-MS/MS) in low binding DNA tubes (Protein LoBind Tubes 1.5 mL; Eppendorf) and homogenized in ice-cold buffer (20 mM Tris pH 8, 20 mM EDTA, 0.1M NaCl, 0.5% NP40) in the ratio 1:9. Homogenization was performed with bead-beating technology using stainless steel balls (Xinxin Stainless steel ball Co., Ltd.) or zirconia bead (Haimen Naisite Experimental Equipment Factory) before snap freezing and storage of homogenate in −80 ± 15°C before analysis. Lung, liver, kidney, and heart were sampled for target knockdown assessment with qPCR by collection of tissue samples submerged in RNAlater solution (Thermo Fisher Scientific) in RNase-free tubes (Thermo Fisher Scientific). The samples were stored overnight at 4°C to allow for penetration of the RNAlater and next transferred to −80 ± 15°C for long-term storage.

Bioanalytical methods

The homogenized tissue samples were analyzed by LC-MS/MS for quantification of the exposure of administered ASOs. Sample preparation was done by liquid-liquid extraction followed by solid phase extraction. The samples were analyzed using a Rack Changer autosampler (Shimadzu) and HPLC system LC30AD (Shimadzu) coupled to an MS/MS instrument AB Sciex API 5500 (AB Sciex, Toronto, Canada) or Shimadzu 8060 (Shimadzu). A gradient was applied over a Waters BEH C18, 130 Å 1.7-μm column (2.1 × 50 mm) (Waters) or a Halo ES-C18 2.7 μ C18 160 Å column (50 × 2.1 mm) (Halo) for chromatographic separation. Mobile phase A was water containing 5% methanol and hexafluoroisopropanol (400 mM) and triethylamin (16 mM) and mobile phase B was 95% methanol containing 5% water.

RNA extraction and quantification

Tissue sections were thawed at room temperature and moved (with an autoclaved tweezer) to a 2 mL Eppendorf tube containing

400 μL lysis buffer (Beckman Coulter Lysis LBE, Cat no C39467) and one 5-mm Stainless steel bead (Qiagen, Cat no 69989). Next, 20 μL proteinase K was added (Beckman Coulter, Cat no C42096) and samples homogenized with an SPEX Sample Prep1600 MiniG, starting at 1,000 RPM for 4 min. Homogenized samples were next incubated for 30 min at 37°C and then placed at −80°C overnight to reduce foam. RNA was finally extracted using an automated protocol on a Biomek i7 (RNAdvance Cell v2, Cat no A47943).

RNA quality and concentration were measured on an Agilent Fragment Analyzer and the amount of input RNA used for cDNA synthesis normalized. cDNA and pre-amplification (12 cycles) was carried out according to the manufacturers recommendations (Fluidigm, Preamp and Reverse Transcription master mix, Cat no 100–6301) and gene expression levels determined using the Biomark HD system (Fluidigm, GE Dynamic Array Reagent Kit, Cat no 100–6267) with the following TaqMan probes (Thermo Fisher Scientific); *Malat1* (Cat no Mm01227912_s1), *Beta-actin,* (Cat no Mm02619580_g1), *Hprt1* (Cat no Mm03024075_m1), and *Rplp0* (Mm00725448_s1).

PK modeling

For the densely sampled concentration-time data, we applied modeling to estimate the tissue half-life and AUC in the target organ. The PK was described by a one-compartmental model with fixed absorption rate of 1 1/h. Numerical analyses were performed in MATLAB (R2020a; The MathWorks). Specifically, the MATLAB function *fminsearch* was used for solving the optimization problems encountered during parameter estimation. Parameter estimation was performed according to a maximum likelihood approach with a proportional error model, using the naive-pooled data approach. For studies with two sampling time points, standard linear regression on logarithmic scale was applied to estimate the tissue half-lives.

Statistical analysis

Tukey's post hoc test was used for multiple comparisons. For data in Figure 3, one-way ANOVA was used. For data in Figure 5, two-way ANOVA for unbalanced design was used. Multiple comparison tests were performed in MATLAB using the functions anova1, anovan, and multcompare. The correlations shown in Figure 4 were performed using GraphPad Prism version 9.4.0 for Windows, GraphPad Software; www.graphpad.com. In all our analyses, p values of less than 0.05 were designated as statistically significant.

DATA AND CODE AVAILABILITY

Data presented in the figures are available in Table S2.

SUPPLEMENTAL INFORMATION

Supplemental information can be found online at https://doi.org/10.1016/j.omtn.2024.102133.

ACKNOWLEDGMENTS

We thank Erika Cavallin for valuable input on the bioanalysis method section. We thank Mattias Bood, Nicola Guzzi, Katya Ribeiro Passos, and Anna Baran for laboratory support.

AUTHOR CONTRIBUTIONS

E.B and P.G. drafted the manuscript. A.B. and P.J. performed the qPCR analysis. All authors critically reviewed and edited the manuscript.

DECLARATION OF INTERESTS

This study was sponsored by AstraZeneca. All authors were employees of AstraZeneca at the time of this research. P.J. is associate editor at *Molecular Therapy Nucleic Acids*.

REFERENCES

1. Chan, J.H.P., Lim, S., and Wong, W.S.F. (2006). Antisense oligonucleotides: from design to therapeutic application. Clin. Exp. Pharmacol. Physiol. *33*, 533–540.
2. Gökirmak, T., Nikan, M., Wiechmann, S., Prakash, T.P., Tanowitz, M., and Seth, P.P. (2021). Overcoming the challenges of tissue delivery for oligonucleotide therapeutics. Trends Pharmacol. Sci. *42*, 588–604.
3. Eckstein, F. (2014). Phosphorothioates, essential components of therapeutic oligonucleotides. Nucleic Acid Therapeut. *24*, 374–387.
4. Hammond, S.M., Aartsma-Rus, A., Alves, S., Borgos, S.E., Buijsen, R.A.M., Collin, R.W.J., Covello, G., Denti, M.A., Desviat, L.R., Echevarría, L., et al. (2021). Delivery of oligonucleotide-based therapeutics: challenges and opportunities. EMBO Mol. Med. *13*, e13243.
5. Crooke, S.T., Liang, X.H., Baker, B.F., and Crooke, R.M. (2021). Antisense technology: A review. J. Biol. Chem. *296*, 100416.
6. Roberts, T.C., Langer, R., and Wood, M.J.A. (2020). Advances in oligonucleotide drug delivery. Nat. Rev. Drug Discov. *19*, 673–694.
7. Geary, R.S. (2009). Antisense oligonucleotide pharmacokinetics and metabolism. Expet Opin. Drug Metabol. Toxicol. *5*, 381–391.
8. Geary, R.S., Norris, D., Yu, R., and Bennett, C.F. (2015). Pharmacokinetics, biodistribution and cell uptake of antisense oligonucleotides. Adv. Drug Deliv. Rev. *87*, 46–51.
9. Peng, B., Andrews, J., Nestorov, I., Brennan, B., Nicklin, P., and Rowland, M. (2001). Tissue distribution and physiologically based pharmacokinetics of antisense phosphorothioate oligonucleotide ISIS 1082 in rat. Antisense Nucleic Acid Drug Dev. *11*, 15–27.
10. Biessen, E.A., Vietsch, H., Rump, E.T., Fluiter, K., Kuiper, J., Bijsterbosch, M.K., and van Berkel, T.J. (1999). Targeted delivery of oligodeoxynucleotides to parenchymal liver cells in vivo. Biochem. J. *340* (Pt 3), 783–792.
11. Prakash, T.P., Graham, M.J., Yu, J., Carty, R., Low, A., Chappell, A., Schmidt, K., Zhao, C., Aghajan, M., Murray, H.F., et al. (2014). Targeted delivery of antisense oligonucleotides to hepatocytes using triantennary N-acetyl galactosamine improves potency 10-fold in mice. Nucleic Acids Res. *42*, 8796–8807.
12. Graham, M.J., Lee, R.G., Brandt, T.A., Tai, L.J., Fu, W., Peralta, R., Yu, R., Hurh, E., Paz, E., McEvoy, B.W., et al. (2017). Cardiovascular and Metabolic Effects of ANGPTL3 Antisense Oligonucleotides. N. Engl. J. Med. *377*, 222–232.
13. Crooke, S.T., Baker, B.F., Xia, S., Yu, R.Z., Viney, N.J., Wang, Y., Tsimikas, S., and Geary, R.S. (2019). Integrated Assessment of the Clinical Performance of GalNAc3-Conjugated 2′-O-Methoxyethyl Chimeric Antisense Oligonucleotides: I. Human Volunteer Experience. Nucleic Acid Therapeut. *29*, 16–32.
14. Hung, G., Xiao, X., Peralta, R., Bhattacharjee, G., Murray, S., Norris, D., Guo, S., and Monia, B.P. (2013). Characterization of target mRNA reduction through in situ RNA hybridization in multiple organ systems following systemic antisense treatment in animals. Nucleic Acid Therapeut. *23*, 369–378.
15. Donner, A.J., Wancewicz, E.V., Murray, H.M., Greenlee, S., Post, N., Bell, M., Lima, W.F., Swayze, E.E., and Seth, P.P. (2017). Co-Administration of an Excipient Oligonucleotide Helps Delineate Pathways of Productive and Nonproductive Uptake of Phosphorothioate Antisense Oligonucleotides in the Liver. Nucleic Acid Therapeut. *27*, 209–220.
16. Geary, R.S., Wancewicz, E., Matson, J., Pearce, M., Siwkowski, A., Swayze, E., and Bennett, F. (2009). Effect of dose and plasma concentration on liver uptake and

pharmacologic activity of a 2′-methoxyethyl modified chimeric antisense oligonucleotide targeting PTEN. Biochem. Pharmacol. *78*, 284–291.

17. Fey, R.A., Templin, M.V., McDonald, J.D., Yu, R.Z., Hutt, J.A., Gigliotti, A.P., Henry, S.P., and Reed, M.D. (2014). Local and systemic tolerability of a 2′O-methoxyethyl antisense oligonucleotide targeting interleukin-4 receptor-alpha delivery by inhalation in mouse and monkey. Inhal. Toxicol. *26*, 452–463.
18. Crosby, J.R., Zhao, C., Jiang, C., Bai, D., Katz, M., Greenlee, S., Kawabe, H., McCaleb, M., Rotin, D., Guo, S., and Monia, B.P. (2017). Inhaled ENaC antisense oligonucleotide ameliorates cystic fibrosis-like lung disease in mice. J. Cyst. Fibros. *16*, 671–680.
19. Moschos, S.A., Frick, M., Taylor, B., Turnpenny, P., Graves, H., Spink, K.G., Brady, K., Lamb, D., Collins, D., Rockel, T.D., et al. (2011). Uptake, efficacy, and systemic distribution of naked, inhaled short interfering RNA (siRNA) and locked nucleic acid (LNA) antisense. Mol. Ther. *19*, 2163–2168.
20. Shin, M., Chan, I.L., Cao, Y., Gruntman, A.M., Lee, J., Sousa, J., Rodríguez, T.C., Echeverria, D., Devi, G., Debacker, A.J., et al. (2022). Intratracheally administered LNA gapmer antisense oligonucleotides induce robust gene silencing in mouse lung fibroblasts. Nucleic Acids Res. *50*, 8418–8430.
21. Beumer, W., Swildens, J., Leal, T., Noel, S., Anthonijsz, H., van der Horst, G., Kuiperij-Boersma, H., Potman, M., van Putten, C., Biasutto, P., et al. (2019). Evaluation of eluforsen, a novel RNA oligonucleotide for restoration of CFTR function in in vitro and murine models of p.Phe508del cystic fibrosis. PLoS One *14*, e0219182.
22. Guimond, A., Viau, E., Aubé, P., Renzi, P.M., Paquet, L., and Ferrari, N. (2008). Advantageous toxicity profile of inhaled antisense oligonucleotides following chronic dosing in non-human primates. Pulm. Pharmacol. Ther. *21*, 845–854.
23. Nicklin, P.L., Bayley, D., Giddings, J., Craig, S.J., Cummins, L.L., Hastewell, J.G., and Phillips, J.A. (1998). Pulmonary bioavailability of a phosphorothioate oligonucleotide (CGP 64128A): comparison with other delivery routes. Pharm. Res. (N. Y.) *15*, 583–591.
24. Yu, R.Z., Kim, T.W., Hong, A., Watanabe, T.A., Gaus, H.J., and Geary, R.S. (2007). Cross-species pharmacokinetic comparison from mouse to man of a second-generation antisense oligonucleotide, ISIS 301012, targeting human apolipoprotein B-100. Drug Metab. Dispos. *35*, 460–468.
25. Crooke, S.T., Vickers, T.A., and Liang, X.H. (2020). Phosphorothioate modified oligonucleotide-protein interactions. Nucleic Acids Res. *48*, 5235–5253.
26. Hagedorn, P.H., Persson, R., Funder, E.D., Albæk, N., Diemer, S.L., Hansen, D.J., Møller, M.R., Papargyri, N., Christiansen, H., Hansen, B.R., et al. (2018). Locked nucleic acid: modality, diversity, and drug discovery. Drug Discov. Today *23*, 101–114.
27. Crooke, R.M., Graham, M.J., Martin, M.J., Lemonidis, K.M., Wyrzykiewiecz, T., and Cummins, L.L. (2000). Metabolism of antisense oligonucleotides in rat liver homogenates. J. Pharmacol. Exp. Therapeut. *292*, 140–149.
28. Karaki, S., Paris, C., and Rocchi, P. (2019). In Antisense Therapy, S. Sharad and S. Kapur, eds. (London: IntechOpen).
29. Basiri, B., Xie, F., Wu, B., Humphreys, S.C., Lade, J.M., Thayer, M.B., Yamaguchi, P., Florio, M., and Rock, B.M. (2020). Introducing an In Vitro Liver Stability Assay Capable of Predicting the In Vivo Pharmacodynamic Efficacy of siRNAs for IVIVC. Mol. Ther. Nucleic Acids *21*, 725–736.
30. Zanardi, T.A., Han, S.C., Jeong, E.J., Rime, S., Yu, R.Z., Chakravarty, K., and Henry, S.P. (2012). Pharmacodynamics and subchronic toxicity in mice and monkeys of ISIS 388626, a second-generation antisense oligonucleotide that targets human sodium glucose cotransporter 2. J. Pharmacol. Exp. Therapeut. *343*, 489–496.
31. Burel, S.A., Han, S.R., Lee, H.S., Norris, D.A., Lee, B.S., Machemer, T., Park, S.Y., Zhou, T., He, G., Kim, Y., et al. (2013). Preclinical evaluation of the toxicological effects of a novel constrained ethyl modified antisense compound targeting signal transducer and activator of transcription 3 in mice and cynomolgus monkeys. Nucleic Acid Therapeut. *23*, 213–227.
32. Yu, R.Z., Gunawan, R., Post, N., Zanardi, T., Hall, S., Burkey, J., Kim, T.W., Graham, M.J., Prakash, T.P., Seth, P.P., et al. (2016). Disposition and Pharmacokinetics of a GalNAc3-Conjugated Antisense Oligonucleotide Targeting Human Lipoprotein (a) in Monkeys. Nucleic Acid Therapeut. *26*, 372–380.
33. Wang, Y., Yu, R.Z., Henry, S., and Geary, R.S. (2019). Pharmacokinetics and Clinical Pharmacology Considerations of GalNAc3-Conjugated Antisense Oligonucleotides. Expet Opin. Drug Metabol. Toxicol. *15*, 475–485.
34. Weidolf, L., Björkbom, A., Dahlén, A., Elebring, M., Gennemark, P., Hölttä, M., Janzén, D., Li, X., and Andersson, S. (2021). Distribution and biotransformation of therapeutic antisense oligonucleotides and conjugates. Drug Discov. Today *26*, 2244–2258.
35. Edwards, A.Y., Elgart, A., Farrell, C., Barnett-Griness, O., Rabinovich-Guilatt, L., and Spiegelstein, O. (2017). A population pharmacokinetic meta-analysis of custirsen, an antisense oligonucleotide, in oncology patients and healthy subjects. Br. J. Clin. Pharmacol. *83*, 1932–1943.
36. Andersson, S., Antonsson, M., Elebring, M., Jansson-Löfmark, R., and Weidolf, L. (2018). Drug metabolism and pharmacokinetic strategies for oligonucleotide- and mRNA-based drug development. Drug Discov. Today *23*, 1733–1745.
37. Nanavati, C., McMullen, G., Yu, R., Geary, R.S., Henry, S.P., and Wang, Y. (2021). Interspecies Scaling of Human Clearance and Plasma Trough Exposure for Antisense Oligonucleotides: A Retrospective Analysis of GalNAc3-Conjugated and Unconjugated-Antisense Oligonucleotides. Nucleic Acid Therapeut. *31*, 298–308.
38. Yu, R.Z., Grundy, J.S., Henry, S.P., Kim, T.W., Norris, D.A., Burkey, J., Wang, Y., Vick, A., and Geary, R.S. (2015). Predictive dose-based estimation of systemic exposure multiples in mouse and monkey relative to human for antisense oligonucleotides with 2′-o-(2-methoxyethyl) modifications. Mol. Ther. Nucleic Acids *4*, e218.